

Ultraviolet Number Counts of Galaxies from *Swift* UV/Optical Telescope Deep Imaging of the Chandra Deep Field South

E. A. Hoversten¹, C. Gronwall¹, D. E. Vanden Berk², T. S. Koch¹, A. A. Breeveld³, P. A. Curran³, D. A. Hinshaw⁴, F. E. Marshall⁴, P. W. A. Roming¹, M. H. Siegel¹, and M. Still³

ABSTRACT

Deep *Swift* UV/Optical Telescope (UVOT) imaging of the Chandra Deep Field South is used to measure galaxy number counts in three near ultraviolet (NUV) filters (uvw2: 1928 Å, uvm2: 2246 Å, uvw1: 2600 Å) and the *u* band (3645 Å). UVOT observations cover the break in the slope of the NUV number counts with greater precision than the number counts by the Hubble Space Telescope (HST) Space Telescope Imaging Spectrograph (STIS) and the *Galaxy Evolution Explorer* (*GALEX*), spanning a range from $21 \lesssim m_{AB} \lesssim 25$. Number counts models confirm earlier investigations in favoring models with an evolving galaxy luminosity function.

Subject headings: galaxies: evolution — galaxies: UV properties — galaxies: number density — Chandra Deep Field South

1. Introduction

Galaxy number counts as a function of magnitude provide direct constraints on galaxy evolution in both luminosity and number density. Number counts in the UV, in particular, can help trace the star formation history of the universe. Until recently obtaining faint galaxy number counts in the UV has been difficult due to the small areas surveyed (Gardner, Brown, & Ferguson 2000; Deharveng et al. 1994; Iglesias-Páramo et al. 2004; Sasseen et al. 2002; Teplitz et al. 2006). While the *Galaxy Evolution Explorer* (*GALEX*) has allowed for the measurement of UV galaxy number counts over a wide field of view (Xu et al. 2005,

¹Department of Astronomy & Astrophysics, The Pennsylvania State University, 525 Davey Laboratory, University Park, PA 16801

²Physics Department, St. Vincent College, Latrobe, PA 15650

³Mullard Space Science Laboratory/UCL, Holmbury St. Mary, Dorking, Surrey RH5 6NT

⁴NASA/Goddard Space Flight Center, Greenbelt, MD 20771

$\sim 20 \text{ deg}^2$), the confusion limit of *GALEX* restricts the magnitude range covered to 14 to 23.8 m_{AB} . The deepest UV number counts from *HST* range from $m_{AB} = 23$ to 29 over an extremely small field of view of ~ 1.3 square arcminutes.

Here, we present galaxy number counts obtained in 3 near UV filters (1928 Å, 2246 Å, 2600 Å) as well as in the u band (3645 Å) obtained using the *Swift* UV/Optical Telescope (UVOT; Roming et al. 2005). Deep exposures were taken of a 289 square arcminute field of view overlapping the Chandra Deep Field South (CDF-S; Giacconi et al. 2002) allowing for the measurement of number counts from $m_{AB} = 21$ to 26. UVOT data covers the break in the slope of the NUV number counts with greater precision than the existing *GALEX* and *HST* number counts. We use the UVOT number counts to explore the evolution of star-forming galaxies out to $z \sim 1$.

2. Data & Analysis

The CDF-S was observed with UVOT, one of three telescopes onboard the *Swift* spacecraft (Gehrels et al. 2004), the primary mission of which is to study gamma-ray bursts (GRB). The UVOT is a 30 cm telescope with f -ratio 12.7 (Roming et al. 2005). It has two grisms and seven broadband filters. The central wavelengths and widths of the uvw2, uvm2, uvw1, and u filters used in this paper can be found in Table 1. For a more detailed discussion of the filters, as well as plots of the responses, see (Poole et al. 2008).

Observations of the CDF-S were made between July 7, 2007 and December 29, 2007. CDF-S images are unbinned with a pixel scale of 0.5 arcseconds. UVOT data processing is described in the UVOT Software Guide¹. The data were processed with a version of the UVOT pipeline in which exposure maps are aspect corrected. This feature is not currently available for data currently in the archive but will appear in future versions of the pipeline. Image files and exposure maps were summed using UVOTIMSUM from the publicly available UVOT FTOOLS (HEASoft 6.6.1)². This involves two flux conserving interpolations of the images, the first to convert from the raw frame to sky coordinates, and the second when summing the images. Bad pixels are known and a correction is applied. UVOT, as is the case with all microchannel plate intensified CCDs, is insensitive to cosmic rays. The maximum exposure time in each filter is given in Table 1.

Because *Swift* is optimized for fast slewing to accomplish its GRB mission, the pointing

¹<http://heasarc.gsfc.nasa.gov/docs/swift/analysis>

²<http://heasarc.gsfc.nasa.gov/docs/software/lheasoft/>

accuracy is of order 1 to 2 arcminutes. In addition the requirement that the solar panels face towards the Sun causes the field of view to rotate over the course of the year. As a result the exposure times vary significantly across the summed images. Exposure maps are nearly uniform in the center but become complicated on the edges. Table 1 gives the area covered where the exposure time is at least 98% of the maximum exposure time in each filter. The 98% value was chosen to maximize the area used in this study while simultaneously maintaining a magnitude limited sample.

The area in each filter covered by the 98% exposure time criterion is shown in Figure 1. For comparison the area covered by the CDF-S, Hubble Ultra Deep Field (Beckwith et al. 2006), and Great Observatories Origins Deep Survey (Giavalisco et al. 2004) is shown by the labeled contours. A false color image of the central region of the CDF-S using the uvw2, uvm2, and uvw1 images is shown in Figure 2.

Photometry was performed using SExtractor (Bertin & Arnouts 1996), a publicly available code designed for the identification and measurement of astrophysical sources in large scale galaxy survey data. A full listing of the SExtractor parameters used is provided in the online version of Table 2. The background map, which measures the local background due to the sky and other sources, was generated internally by SExtractor. To improve the detectability of faint extended sources the filtering option was used with a Gaussian filter. The filter size was selected to match the full width half maximum (FWHM) of the point spread function (PSF) as recommended in the SExtractor manual. The PSF was measured from the CDF-S image for each filter using one star. There was only one star which was bright enough and isolated enough to accurately measure the outer regions of the PSF. The PSFs used were 3.30" in uvw2, 2.87" in uvm2, 2.86" in uvw1, and 2.67" in u . Magnitudes were calculated from `MAG_AUTO` which is designed to be the best measure of the total magnitudes of galaxies. SExtractor was used to process count rate images created by dividing the summed images by the exposure map. The resulting output was converted to flux using the values given by Poole et al. (2008) for stellar spectra. The fluxes were then converted to AB magnitudes (Oke 1974). The number of sources detected in each band ranges from 888 to 1260 and is given in Table 1 along with the area covered in each image.

The UVOT detector is a microchannel plate intensified CCD which operates in photon counting mode. As such it is subject to coincidence loss which occurs when two or more photons arrive at a the same location on the detector within a single CCD readout interval of 11 ms (Fordham, Moorhead, & Galbraith 2000). When this happens only one photon will be counted, which systematically undercounts the true number of photons. The coincidence loss correction is at the 1% level for $m_{AB} \sim 19$ in the UVOT filters we use in this paper. For the magnitude ranges considered in our number counts the coincidence loss is insignificant

and no attempts are made to correct for it.

By design the CDF-S is on a line of sight with very low Galactic extinction. In addition the area covered by the UVOT observation is around 130 square arcminutes, depending on the filter, so variations in extinction across the field are small. According to the dust maps of Schlegel, Finkbeiner, & Davis (1998) the range of Galactic extinction in our field is $0.020 \leq A_V \leq 0.030$. Our photometry is corrected for Galactic extinction based on the position of the source assuming the Milky Way dust curve of Pei (1992). The extinction correction is largest in the uvm2 filter as it is centered on the 2175 Å dust feature which is pronounced in the Milky Way. The extinction correction ranges from $0.053 \leq A_{\text{uvm2}} \leq 0.086$ across the field in uvm2 which demonstrates that the extinction correction is not a significant source of error in any of the filters.

3. Bias Corrections

The raw number counts suffer from several biases which need to be quantified. Completeness addresses the inability to detect an object either due to confusion with other sources or limitations in the photometry. Eddington bias (Eddington 1913) occurs because magnitude errors will preferentially scatter objects into brighter magnitude bins because there are generally more objects at fainter magnitudes. There is also the potential for false detections of objects due to noise.

These first two problems can be addressed simultaneously with a Monte Carlo simulation, following the procedure set out in Smail et al. (1995). For each of the four images, synthetic galaxies were added and the analysis repeated. Synthetic galaxies were placed at random locations on the image. The magnitudes of the synthetic galaxies were between 21 and 27 in uvw2, uvm2 and uvw1 and between 20 and 25.5 in u and the relative numbers by magnitude follow the observed distribution from the original SExtractor photometry in the relevant filter. The synthetic galaxies are given exponential profiles with semi-major axes and ellipticities that match the observed distribution as a function of magnitude. Individual photon arrivals are modeled using Poisson statistics and following the galaxy profile. The resulting image is then convolved with the UVOT PSF for the final image.

For each filter a single synthetic galaxy was added to the real image and the photometry process described in §2 was redone. The resulting photometry catalog was checked to determine if the synthetic galaxy was detected and at what magnitude. This was repeated 50,000 times for each filter to build up statistics on the completeness. The number counts were corrected by dividing by the fraction of synthetic galaxies detected in the relevant mag-

nitude bin. These values are tabulated in Table 3. Following Smail et al. (1995) the number counts are truncated where the completeness correction exceeds 50%. The Poisson error bars on the number counts are also divided by the completeness correction to take into account uncertainties introduced by the completeness correction.

Correcting for false detections was also done using the methods of Smail et al. (1995). Using the exposure time and background count rate calculated from the background map output by SExtractor noise frames were simulated for each filter. The photometry methods described in §2 were repeated for each frame and the number of false detections recorded as a function of magnitude. For each filter 100 noise frames were analyzed. The number of spurious sources, N_{spur} , is shown as a function of magnitude for each filter in Table 3. Out of all the simulated frames only one spurious source was detected. Given our deep exposures the completeness correction truncates our number counts well before background noise becomes an issue.

Galaxy number counts can be overestimated due to contamination by Galactic stars and quasars. The fraction of objects in the field that are quasars is estimated by position matching the four UVOT photometry catalogs with the Extended Chandra Deep Field South X-ray point source catalog (Lehmer et al. 2005). Objects with X-ray detections are assumed to be quasars. The number of such sources in each band is 11, 11, 14, and 21 for the uvw2, uvm2, uvw1, and u bands respectively. This represents 1.2, 1.0, 1.1, and 2.3% of the total sample. These sources have been removed from the number counts. The number of AGN per magnitude bin, N_{AGN} , is tabulated in Table 3.

The problem of stellar contamination is greatly reduced by the fact that the line of sight towards the CDF-S is out of the plane of the Milky Way. The CDF-S field was explicitly chosen to be particularly sparse. As a result the field is a statistical outlier, and the stellar contamination in this field will be unusually low. In addition, the fraction of stars with significant UV flux is low, particularly when the field points toward the Galactic halo where the stellar population is very old. This is another reason the stellar contamination in the three NUV filters should be low.

The contamination due to stars is estimated by position matching the UVOT photometry catalogs with objects in the field with stellar classifications in the COMBO-17 survey (Wolf et al. 2004). The COMBO-17 survey includes photometry in 17 passbands for a 30×30 arcminute field surrounding the CDF-S. It also contains photometric redshifts and classifications of objects in the survey. The UVOT positions were compared with the objects classified as stars or white dwarfs in COMBO-17. This yields 24, 15, and 40 stars in the uvw2, uvm2, and uvw1 NUV filters which corresponds to 2.7, 1.4, and 3.2% of the total sample. The number of stars per magnitude bin, N_{star} is shown in Table 3. Not all NUV

number counts are corrected for stellar contamination (e.g. Gardner et al. 2000). Given the numbers provided in Table 3 the number counts can easily be recalculated without the stellar contamination correction.

However it is different in the u band where more stars have significant fluxes. Position matching yielded 48 stars in the u band which is 5.1% of the total sample. As in the NUV counts the stellar contamination has been corrected for and the details are in Table 3. Capak et al. (2004) provide both raw number counts and the number counts corrected for stellar contamination in the U band from observations around the Hubble Deep Field North (HDFN). The u and U filters are comparable, and the HDFN is similar to the CDF-S in being one of the darkest areas of the sky pointed out of the Galactic disk with low Galactic extinction. The level of stellar contamination in Capak et al. (2004) ranges from 66% at $u = 20$ to 6% at $u = 25$. At the bright end of this scale the values are comparable, but at the faint end they are roughly twice as high as in the CDF-S. One possible explanation for this discrepancy is that the Capak et al. (2004) sample covers ~ 720 arcsec² compared to 137 arcsec² for this sample. Over this larger area one would expect the number of stars to be closer to the average number expected for that line of sight to the halo, while in our relatively smaller area the number of stars can remain a statistical outlier.

Cosmic variance is another potential source of bias which arises due to local inhomogeneities in the Universe. Galaxies are known to cluster on many different length scales. As a result the density of galaxies will differ along different lines of sight. The smaller the area covered by a survey the more the results will be biased by cosmic variance. A publicly available code from Trenti & Stiavelli (2008) was used to estimate the errors due to cosmic variance in our number counts. This code is based in part on N -body simulations of galaxy structure formation. It uses the area of the survey, mean redshift, range of redshifts observed and the number of objects detected to calculate the error due to cosmic variance. The mean redshift and redshift range of each of our luminosity bins was estimated from the model number counts described in §4. The results show that the uncertainty due to cosmic variance are of the same order as the Poisson errors for all of the filters and magnitude bins used here. We therefore multiply our Poisson errors by a factor of $\sqrt{2}$ to take into account the effects of cosmic variance.

The resulting corrected number counts are shown in Figures 3 (uvw2), 4 (uvm2), 5 (uvw1), and 6 (u). The number counts are also given in Table 3. In Figures 3, 4, and 5 the number counts are plotted along side the NUV number counts from GALEX (Xu et al. 2005) and STIS (Gardner et al. 2000). A color conversion has been applied to shift the GALEX NUV filter and STIS F25Q7Z filter in the NUV channel by generating synthetic magnitudes from a catalog of spectral synthesis models with a range of ages and star formation histories

and estimating the typical color offset. The GALEX and STIS NUV filters have very similar bandpasses which typically differ by less than 0.01 magnitudes. The uvm2 filter has the tightest relationship with the NUV filters with a color correction of 0.013. The spread is larger in the uvw2 and uvw1 filters, but is still only of order 0.05. In Figure 6 the UVOT u band number counts are compared to the U band counts of Capak et al. (2004) and Eliche-Moral et al. (2006) and the u band measurements of Metcalfe et al. (2001) and Yasuda et al. (2001). Color corrections to the UVOT u band were determined in the same fashion and are equal to 0.81 in U and 0.06 in u .

4. Models

Simple models of number counts were constructed for both non-evolving and evolving luminosity functions in the UVOT filters. For each model the luminosity function is summed over redshift. This summation includes two corrections. The first is a filter correction to convert the GALEX NUV filter to the UVOT uvw2, uvm2, and uvw1 filters and the U band to the UVOT u filter. The second is a K -correction to convert the observed UVOT filter to the rest-frame UVOT filter. Both of these corrections are a function of redshift.

These corrections were calculated using a model galaxy spectrum generated with the publicly available PÉGASE spectral synthesis code (Fioc & Rocca-Volmerange 1997). For the uvw2, uvm2, and uvw1 filters a starburst galaxy model was used with a constant star formation rate, Solar metallicity, and standard Salpeter IMF at an age of 800 Myr. This was chosen to match the model number counts in Xu et al. (2005) which used the SB4 starburst template of Kinney et al. (1996) because it most closely matched the ratio of the local FUV to NUV luminosity densities described by Wyder et al. (2005). The PÉGASE model is very nearly the SB1 template of Kinney et al. (1996), however we model a range of internal extinctions. An $\Omega_M = 0.3$, $\Omega_\Lambda = 0.7$, $H_0 = 70 \text{ km s}^{-1} \text{ Mpc}^{-1}$ cosmology is used throughout.

The u band models were calculated assuming the cosmic spectrum of Baldry et al. (2002) in addition to the starburst spectrum. The cosmic spectrum is a luminosity weighted average spectrum of galaxies with $z \lesssim 0.1$ which makes it a good choice for a template representative of all galaxies. The empirical cosmic spectrum does not extend far enough into the blue to be useful for modeling the UVOT u band let alone passing it through the filters at increasing redshifts. To extend the spectrum into the ultraviolet a template spectrum was created in PÉGASE from the best fitting parameters given by Baldry et al. (2002). The model number counts were corrected for a range of models of internal extinction. Models were calculated for $0 \leq A_V \leq 2$ for the Milky Way, LMC, and SMC dust models of Pei (1992) and the starburst dust model of Calzetti, Kinney, & Storchi-Bergmann (1994).

Galaxy luminosity functions have traditionally been fit empirically using Schechter functions (Schechter 1976). The Schechter function is given by

$$\phi(M)dM = \frac{\ln 10}{2.5} \phi^* [10^{0.4(M^*-M)}]^{\alpha+1} \exp [-10^{0.4(M^*-M)}] dM \quad (1)$$

where $\phi(M)dM$ is the number of galaxies with absolute magnitude between M and $M + dM$ per Mpc^3 . Three free parameters are fit using an empirical luminosity function; α is the slope at the faint end of the luminosity function, M^* is the luminosity where the luminosity function turns over, and ϕ^* is the density normalization.

For the non-evolving models the local galaxy luminosity function was used at all redshifts. The GALEX NUV galaxy luminosity function of Wyder et al. (2005) was used for the uvw2, uvm2, and uvw1 models. In the u band the models are based on the local U band luminosity function from Ilbert et al. (2005). In the evolving models the Schechter function parameters α , ϕ^* , and M^* vary with redshift. In the uvw2, uvm2, and uvw1 bands the evolution of the Schechter function parameters is based on their evolution at 1500 \AA as found by Arnouts et al. (2005), normalized to match the Wyder et al. (2005) NUV parameters for the local universe. For the u band the evolution of the Schechter function parameters comes from Ilbert et al. (2005). In neither the non-evolving nor evolving models does the dust extinction change as a function of redshift, nor does the underlying galaxy template evolve. A model with that level of complexity would be beyond the scope of this paper.

The model number counts are also corrected for the Lyman forest and continuum using the methods described by Madau (1995). With the exception of Hubble Deep Field U band number counts (Metcalf et al. 2001; Volonteri et al. 2000) NUV and U model number counts are generally not corrected for Lyman absorption. Our modeling reveals that this is justified. In the bands considered in this paper this affects the models by a few percent at 29th magnitude and much less at brighter magnitudes. Although the models described here are plotted mainly for context the Lyman absorption corrections are included.

Example models are plotted with the number counts in Figures 3, 4, 5, and 6.

5. Results

Figures 3 and 4 show that in the uvw2 and uvm2 filters the number counts are in excellent agreement with the NUV results from GALEX (Xu et al. 2005) and HST (Gardner et al. 2000). Furthermore, Figures 3 and 4 demonstrate the unique contribution of UVOT. The UVOT number counts have a significant overlap with GALEX, however they continue ~ 1.5 magnitudes deeper with error bars comparable to those of GALEX. In this magnitude

range they overlap with the HST number counts, but are much less uncertain due to the wider field of view of UVOT as compared to STIS. While UVOT is not able to go as deep as HST, it provides more precise number counts in the magnitude range where there is a knee in the slope of the number counts.

Figures 3 and 4 also show some of the models discussed in §4. The models shown are for the star forming galaxy template with Calzetti et al. (1994) dust models and $A_V = 1.0$. The solid line is a model with a non-evolving galaxy luminosity function and the dashed line is an evolving model following the evolution of the Schechter function parameters described by Arnouts et al. (2005). The underlying models are the same in the two figures, but have been calculated for the different filters. In both cases the non-evolving luminosity function model under-predicts the number counts given the galaxy template and extinction assumptions. However the evolving luminosity function model is simultaneously in good agreement with the uvw2 and uvm2 number counts. This is an independent confirmation that the evolution in the luminosity function parameters found by Arnouts et al. (2005) are reasonable.

Figure 5 shows that the uvw1 number counts are significantly higher than the GALEX NUV counts. This can be explained by the fact that the uvw1 filter has a tail in the red with significant sensitivity between 3000 and 4000 Å. This extends redward of the limits of the GALEX and STIS NUV filters. At this point bright elliptical galaxies can be detected in spite of the fact that they do not produce an appreciable flux in the NUV. Beyond the extreme case of ellipticals, post-starburst galaxies with substantial populations of A type stars and even to a lesser extent regular spiral galaxies will also be over represented in the uvw1 number counts compared to the NUV due to light being detected in the red wing of the uvw1 filter.

The black models in Figure 5 are the same as those in Figures 3 and 4. The evolving luminosity function model is still better than the no evolution model, and is fairly representative of the GALEX and HST number counts. However it does not agree with the uvw1 number counts as well as in the uvw2 and uvm2. This is due to the fact that the starburst galaxy template is too blue to take into account the red objects which may be detected by the red end of the uvw1 filter. The red models assume the same evolutionary parameters as the black models but uses the redder cosmic spectrum of Baldry et al. (2002) as the galaxy template. The models using the cosmic spectrum template are below their respective star forming template counterparts. Thus the cosmic spectrum model has the opposite problem in that it undercounts galaxies experiencing strong star formation. This shows that the simple modeling used here is less successful for describing the uvw1 number counts, but also suggests that the uvw1 filter could be useful in constraining the relative numbers of different galaxy types over time.

Figure 6 shows that the u band number counts are generally in good agreement with other observations. On the faint end of the number counts the UVOT observations are in excellent agreement with the U band counts of Capak et al. (2004) and Eliche-Moral et al. (2006) and the u band counts of Metcalfe et al. (2001). At around magnitude 22 to 23 the UVOT number counts appear about 50% higher. One explanation for this is that the Yasuda et al. (2001) u number counts are also higher than the other observations on the faint end. Modeling galaxy colors shows that the SDSS u is a much better proxy for UVOT u than Johnson U . The higher number counts may be due to additional blue sensitivity. Figure 6 also reveals that in the u band UVOT does not have the unique advantage it has in the NUV filters as it covers the same magnitude range as the ground based observations and does not go as deep. However it provides an independent check on the ground based results.

Figure 6 also shows u band model number counts for both the starburst (black) and cosmic spectrum (red) templates, and both non-evolving luminosity functions (solid) and those which evolve with the parameters of Ilbert et al. (2005). In the u band the evolving luminosity function models with the starburst and cosmic spectrum templates bracket the observed number counts, but then turn over at $u \sim 25$ faster than the observed counts.

In summary, the UVOT is uniquely positioned to cover the knee in the galaxy number counts compared to GALEX and HST in the NUV. Due to its smaller PSF it can go deeper than the GALEX confusion limit, and its larger field of view provides better statistics on the bright end of the STIS number counts. The simple model number counts used here strongly point to an evolving galaxy luminosity function in agreement with earlier studies. More detailed models are needed to explain the number counts in the uvw1 and u filters, but are beyond the scope of this paper. However the measurements provided by this paper in the magnitude range where the number counts turn over will enable a more precise differentiation between models. In addition, the three NUV filters of UVOT are narrower than the single NUV filter of STIS and GALEX so more color information is provided which is potentially useful for more involved modeling. Future plans include measurements of the UV galaxy luminosity function as a function of redshift.

We acknowledge support from NASA Astrophysics Data Analysis grant, #NNX09AC87G. This work is sponsored at PSU by NASA contract NAS5-00136 and at MSSL by funding from the Science and Technology Facilities Council (STFC).

Facilities: Swift (UVOT)

REFERENCES

- Arnouts, S., et al. 2005, ApJ, 619, L43
- Baldry, I. K., et al. 2002, ApJ, 569, 582
- Beckwith, S. V. W., et al. 2006, AJ, 132, 1729
- Bertin, E. & Arnouts, S. 1996, A&AS, 117, 393
- Calzetti, D., Kinney, A. L., & Storchi-Bergmann, T. 1994, ApJ, 429, 582
- Capak, P., et al. 2004, AJ, 127, 180
- Deharveng, J.-M., et al. 1994, A&A, 289, 715
- Eddington, A. S. 1913, MNRAS, 73, 359
- Eliche-Moral, M. C., et al. 2006, ApJ, 639, 644
- Fioc, M. & Rocca-Volmerange, B. 1997, A&A, 326, 950
- Fordham, J. L. A., Moorhead, C. F., & Galbraith, R. F. 2000, MNRAS, 312, 83
- Gardner, J. P., Brown, T. M., & Ferguson, H. C. 2000, ApJ, 542, L79
- Gehrels, N., et al. 2004, ApJ, 611, 1005
- Giacconi, R., et al. 2002, ApJS, 139, 369
- Giavalisco, M., et al. 2004, ApJ, 600, L93
- Iglesias-Páramo, J., et al. 2004, A&A, 419, 109
- Ilbert, O., et al. 2005, A&A, 439, 863
- Kinney, A. L., et al. 1996, ApJ, 467, 38
- Lehmer, B. D., et al. 2005, ApJS, 161, 21
- Madau, P. 1995, ApJ, 441, 18
- Metcalfe, N., et al. 2001, MNRAS, 323, 795
- Oke, J. B. 1974, ApJS, 27, 21
- Pei, Y. C. 1992, ApJ, 395, 130

Poole, T. S., et al. 2008, MNRAS, 383, 627

Roming, P. W. A., et al. 2005, Space Science Reviews, 120, 95

Sasseen, T. P., et al. 2002, ArXiv Astrophysics e-prints

Schechter, P. 1976, ApJ, 203, 297

Schlegel, D. J., Finkbeiner, D. P., & Davis, M. 1998, ApJ, 500, 525

Smail, I., et al. 1995, ApJ, 449, L105+

Teplitz, H. I., et al. 2006, AJ, 132, 853

Trenti, M. & Stiavelli, M. 2008, ApJ, 676, 767

Volonteri, M., et al. 2000, A&A, 362, 487

Wolf, C., et al. 2004, A&A, 421, 913

Wyder, T. K., et al. 2005, ApJ, 619, L15

Xu, C. K., et al. 2005, ApJ, 619, L11

Yasuda, N., et al. 2001, AJ, 122, 1104

This preprint was prepared with the AAS L^AT_EX macros v5.2.

Table 1. *Swift* UVOT observations of the CDF-S

Filter	Central Wavelength (Å)	FWHM (Å)	Exposure (s)	Area (arcmin ²) ^a	# Sources
uvw2	1928	657	144763	132.7	888
uvm2	2246	498	136286	112.0	1061
uvw1	2600	693	158334	143.2	1260
u	3465	785	124787	136.6	931

^aArea used for number counts where the exposure time is greater than or equal to 98% of the maximum exposure time at the center of the image.

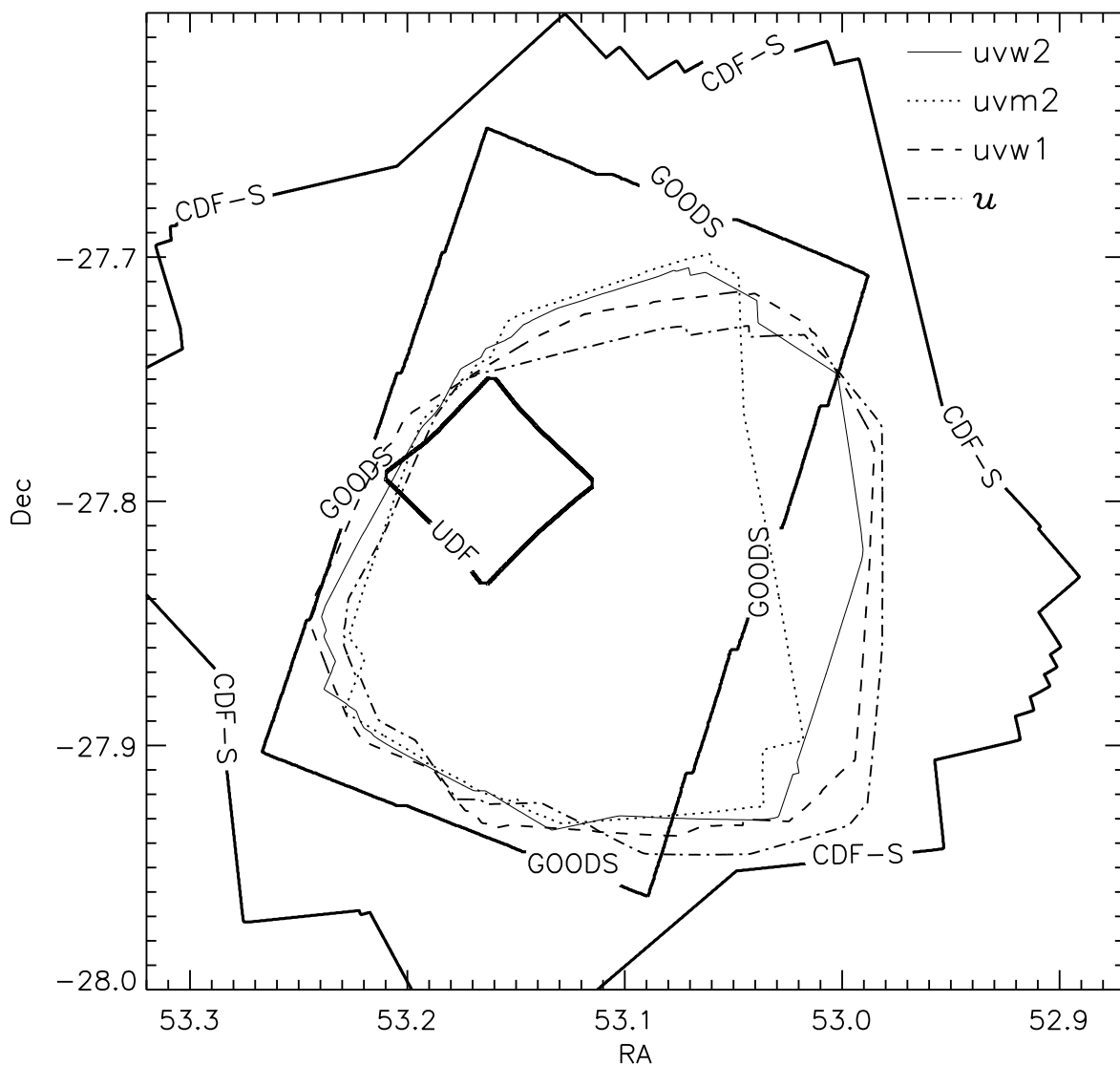


Fig. 1.— Field of view for UVOT CDF-S observations. Contours indicate the area covered with at least 98% of the maximum exposure time as described in the text and tabulated in Table 1. The contours are uvw2 (thin solid line), uvm2 (dotted line), uvw1 (dashed line), and u (dot-dashed line). For reference the extent of the Chandra Deep Field South (Giacconi et al. 2002), Hubble Ultra Deep Field (Beckwith et al. 2006) and Great Observatories Origins Deep Survey (Giavalisco et al. 2004) are denoted by thick contours which are labeled.



Fig. 2.— Synthetic color image of a portion of the UVOT CDF-S deep field. This image includes uvw2 (blue), uvm2 (green), and uvw1 (red). The u band is not included in the image. For reference the green bar is 1 arcminute long.

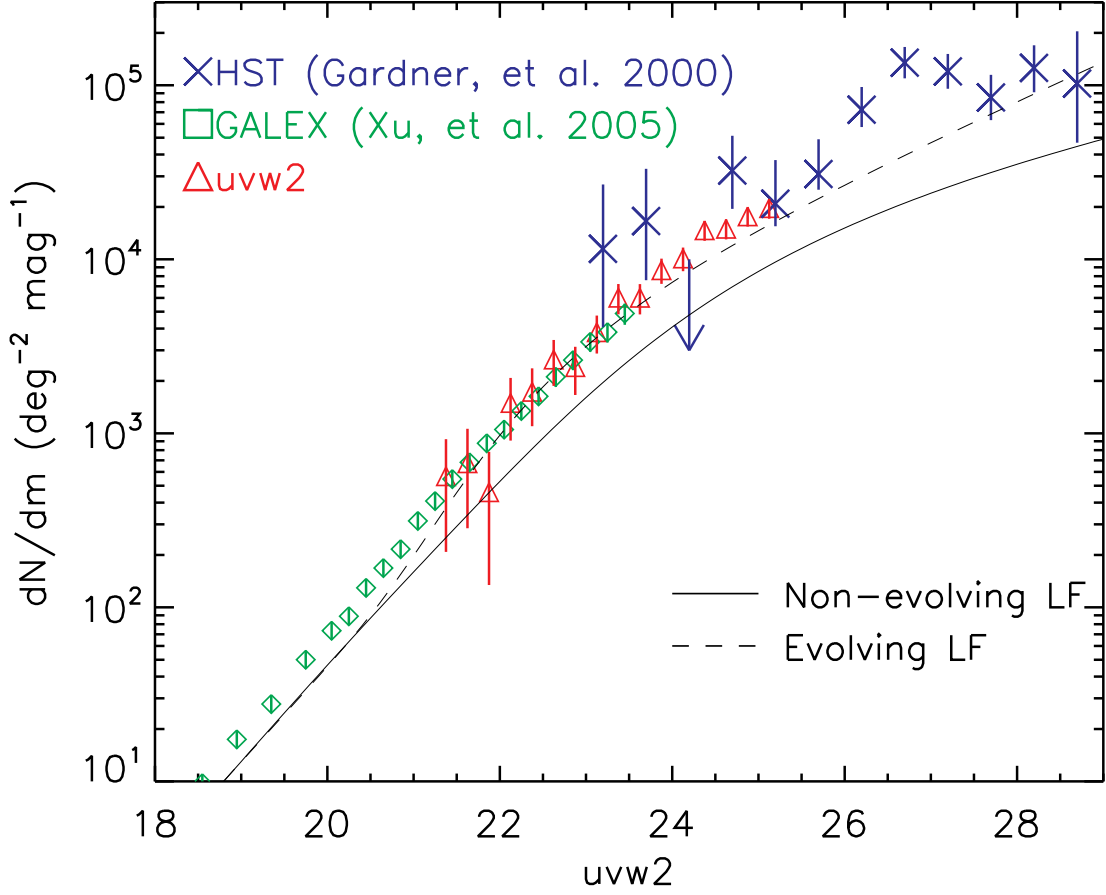


Fig. 3.— UV number counts in the uvw2 filter (red triangles). GALEX NUV number counts (Xu et al. 2005, green diamonds), and STIS NUV number counts Gardner et al. (2000, blue X’s) are also plotted with a conversion to the uvw2 filter as described in the text. Model number counts are also plotted for a starburst template galaxy and Calzetti et al. (1994) dust model with $A_V = 1$ and galaxy luminosity function parameters from Wyder et al. (2005). Models for a non-evolving (solid line) and an evolving (dashed line) galaxy luminosity function following Arnouts et al. (2005) are shown.

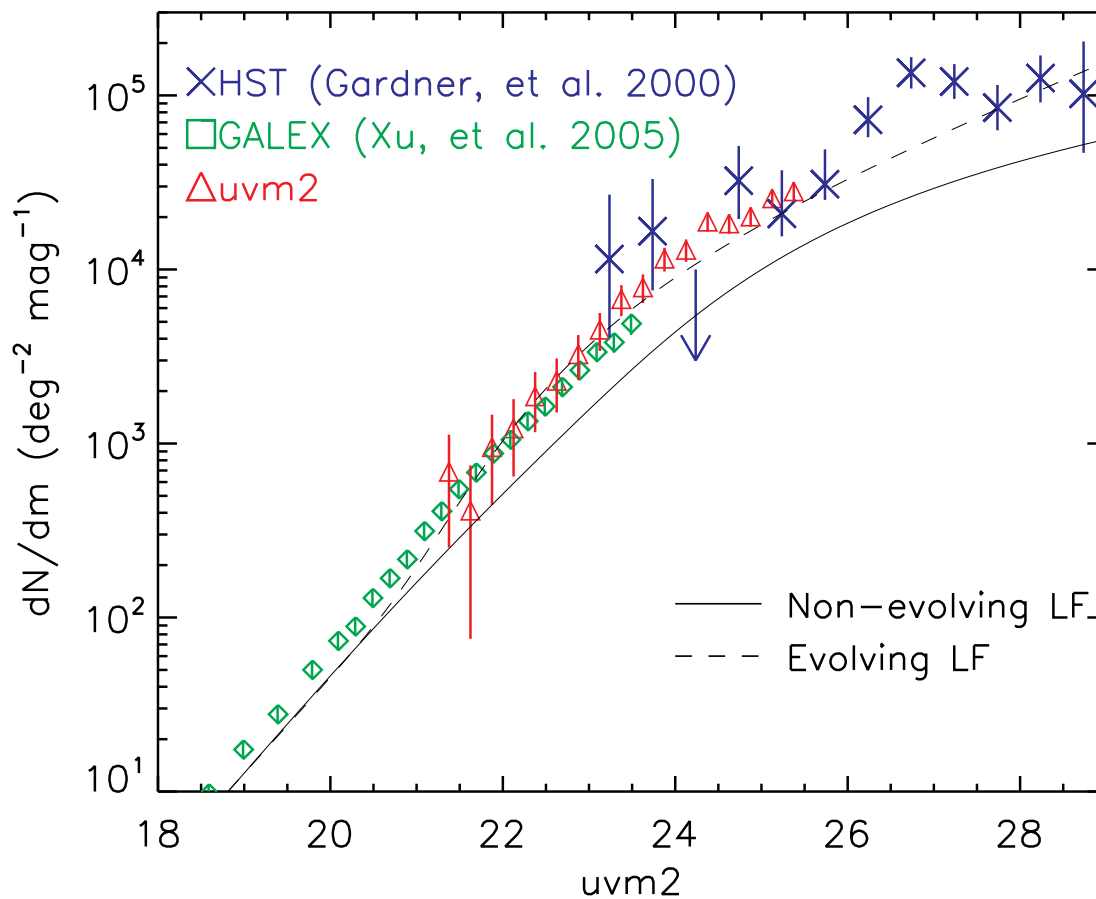


Fig. 4.— UV number counts in the uvm2 filter (red triangles). The rest of the description follows Figure 3.

Table 2. SExtractor parameters for CDF-S photometry

Parameter Name	Parameter Value
ANALYSIS_THRESH	5.0

Note. — Table 2 appears in its entirety in the online version of the *Astrophysical Journal*. A portion is provided here for guidance regarding its form and content.

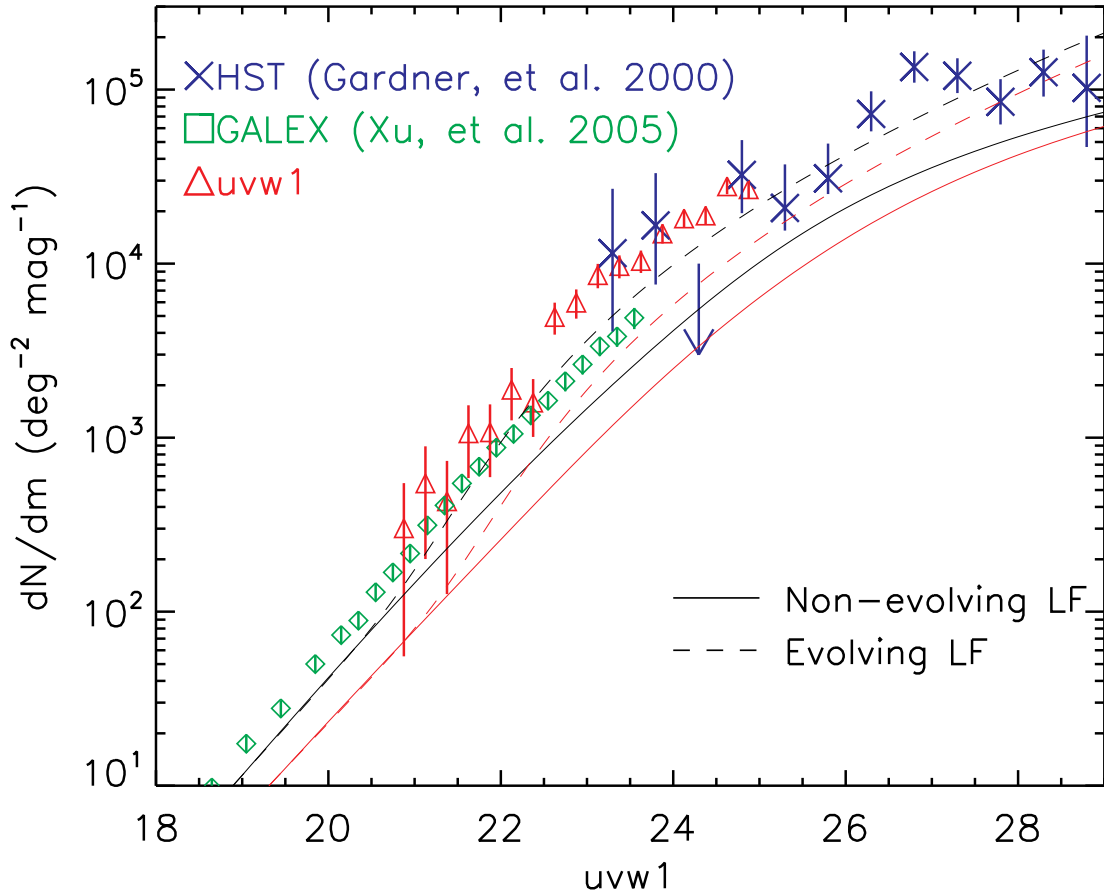


Fig. 5.— UV number counts in the $uvw1$ filter (red triangles). In addition to the description from Figure 3, model number counts assuming the cosmic spectrum of Baldry et al. (2002) as a template are shown in red for both non-evolving (solid line) and evolving (dashed line) luminosity functions.

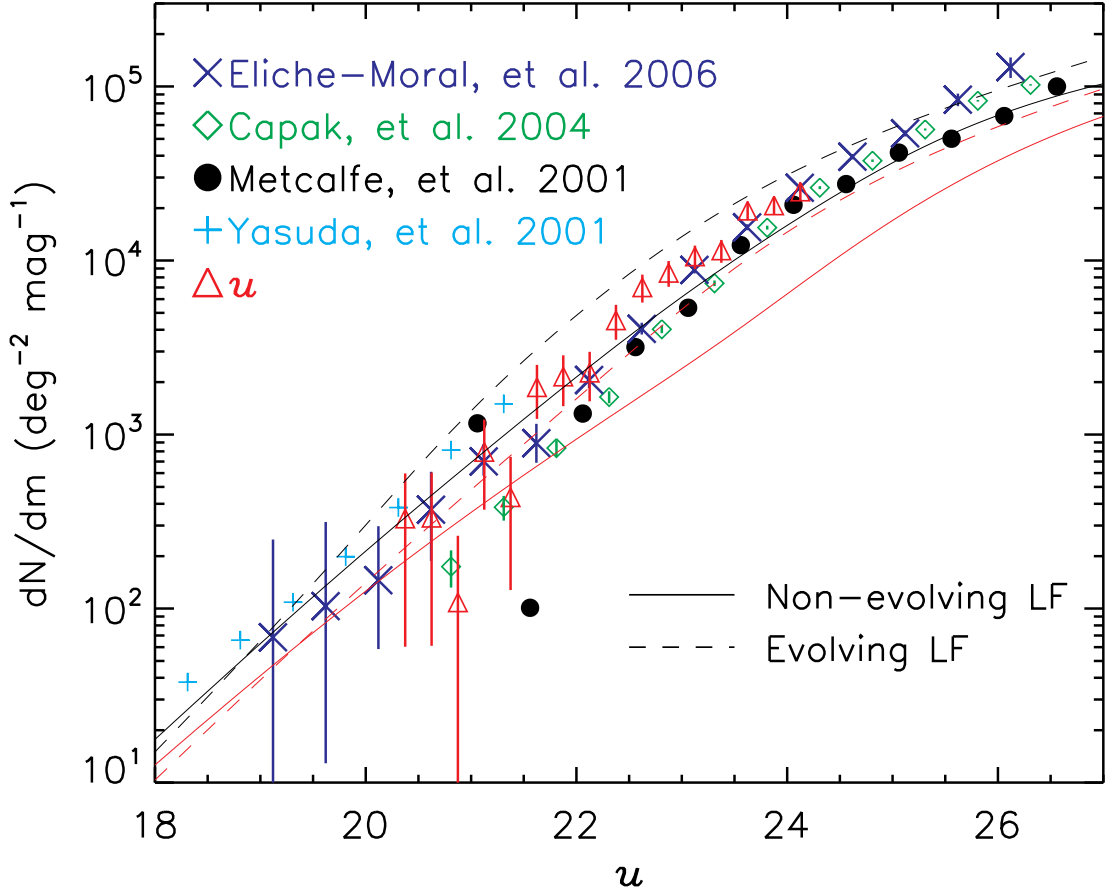


Fig. 6.— Galaxy number counts in the UVOT u filter (red triangles). U number counts from Capak et al. (2004) (green diamonds), Eliche-Moral et al. (2006) (blue X's), and Metcalfe et al. (2001) (black circles), as well as SDSS u number counts from Yasuda et al. (2001) (cyan plus signs) are also plotted with a conversion to the UVOT u filter as described in the text. Yasuda et al. (2001) and Metcalfe et al. (2001) do not tabulate their errors. Model number counts are also plotted for a starburst template galaxy and Calzetti et al. (1994) dust model with $A_V = 1$, and galaxy luminosity function parameters from Ilbert et al. (2005) are shown in black for non-evolving (solid line) and an evolving (dashed line) galaxy luminosity functions. Model number counts assuming the cosmic spectrum of Baldry et al. (2002) as a template are shown in red for both non-evolving (solid line) and evolving (dashed line) luminosity functions.

Table 3. *Swift* UVOT galaxy number counts in the CDF-S

m_{AB}	Filter	Counts (deg ⁻² mag ⁻¹)	N_{raw}	N_{stars}	N_{AGN}	N_{spur}	Completeness	Area (arcmin ²)
21.375	uvw2	566 ± 358	7	2	0	0.00	0.957	132.708
21.625	uvw2	673 ± 388	6	0	0	0.00	0.967	132.708
21.875	uvw2	458 ± 324	4	0	0	0.00	0.946	132.708
22.125	uvw2	1494 ± 586	14	1	0	0.00	0.944	132.708
22.375	uvw2	1731 ± 632	17	2	0	0.00	0.940	132.708
22.625	uvw2	2656 ± 783	24	1	0	0.00	0.940	132.708
22.875	uvw2	2401 ± 741	21	0	0	0.00	0.949	132.708
23.125	uvw2	3811 ± 938	36	3	0	0.00	0.939	132.708
23.375	uvw2	6018 ± 1191	56	2	3	0.00	0.919	132.708
23.625	uvw2	6011 ± 1190	52	0	1	0.00	0.921	132.708
23.875	uvw2	8655 ± 1432	76	2	1	0.00	0.915	132.708
24.125	uvw2	10108 ± 1569	89	4	2	0.00	0.891	132.708
24.375	uvw2	14694 ± 1921	117	0	0	0.00	0.864	132.708
24.625	uvw2	14980 ± 1967	122	5	1	0.00	0.840	132.708
24.875	uvw2	17648 ± 2223	129	1	2	0.00	0.775	132.708
25.125	uvw2	19683 ± 2584	118	1	1	0.00	0.639	132.708
21.375	uvm2	687 ± 435	5	0	0	0.00	0.943	110.982
21.625	uvm2	411 ± 335	3	0	0	0.00	0.946	110.982
21.875	uvm2	953 ± 509	7	0	0	0.00	0.952	110.982
22.125	uvm2	1221 ± 575	12	3	0	0.00	0.956	110.982
22.375	uvm2	1866 ± 705	14	0	0	0.00	0.973	110.982
22.625	uvm2	2293 ± 786	17	0	0	0.00	0.962	110.982
22.875	uvm2	3259 ± 940	26	2	0	0.00	0.955	110.982
23.125	uvm2	4510 ± 1110	35	1	1	0.00	0.949	110.982
23.375	uvm2	6757 ± 1365	49	0	0	0.00	0.941	110.982
23.625	uvm2	7894 ± 1478	58	1	0	0.00	0.937	110.982
23.875	uvm2	11535 ± 1801	82	0	0	0.00	0.922	110.982
24.125	uvm2	12975 ± 1913	94	2	0	0.00	0.920	110.982
24.375	uvm2	18846 ± 2337	130	0	0	0.00	0.895	110.982
24.625	uvm2	18397 ± 2336	125	0	1	0.00	0.875	110.982
24.875	uvm2	20142 ± 2537	131	2	3	0.00	0.812	110.982
25.125	uvm2	25642 ± 3022	147	1	2	0.00	0.729	110.982
25.375	uvm2	28135 ± 3647	126	3	4	0.00	0.549	110.982
20.875	uvw1	301 ± 246	3	0	0	0.00	1.000	143.192
21.125	uvw1	545 ± 345	6	1	0	0.00	0.921	143.192
21.375	uvw1	430 ± 304	6	2	0	0.00	0.934	143.192
21.625	uvw1	1060 ± 474	13	3	0	0.00	0.948	143.192
21.875	uvw1	1073 ± 479	13	3	0	0.00	0.937	143.192
22.125	uvw1	1885 ± 628	19	0	1	0.00	0.960	143.192
22.375	uvw1	1590 ± 580	18	2	1	0.00	0.948	143.192
22.625	uvw1	4935 ± 1029	50	4	0	0.00	0.937	143.192
22.875	uvw1	5968 ± 1138	56	1	0	0.00	0.927	143.192
23.125	uvw1	8594 ± 1376	81	2	1	0.00	0.913	143.192
23.375	uvw1	9689 ± 1460	90	2	0	0.00	0.913	143.192
23.625	uvw1	10364 ± 1519	98	3	2	0.00	0.902	143.192

Table 3—Continued

m_{AB}	Filter	Counts (deg ⁻² mag ⁻¹)	N_{raw}	N_{stars}	N_{AGN}	N_{spur}	Completeness	Area (arcmin ²)
23.875	uvw1	14905 ± 1863	134	4	2	0.00	0.864	143.192
24.125	uvw1	18182 ± 2092	154	3	0	0.00	0.835	143.192
24.375	uvw1	18908 ± 2190	157	5	3	0.00	0.792	143.192
24.625	uvw1	27819 ± 2775	206	3	2	0.00	0.727	143.192
24.875	uvw1	26781 ± 3072	156	2	2	0.00	0.571	143.192
20.375	<i>u</i>	328 ± 268	5	2	0	0.00	0.962	136.569
20.625	<i>u</i>	332 ± 271	5	2	0	0.00	0.951	136.569
20.875	<i>u</i>	108 ± 153	4	3	0	0.00	0.972	136.569
21.125	<i>u</i>	794 ± 424	9	2	0	0.00	0.930	136.569
21.375	<i>u</i>	436 ± 308	4	0	0	0.00	0.967	136.569
21.625	<i>u</i>	1871 ± 642	22	5	0	0.00	0.958	136.569
21.875	<i>u</i>	2154 ± 699	21	2	0	0.00	0.930	136.569
22.125	<i>u</i>	2269 ± 717	24	3	1	0.00	0.929	136.569
22.375	<i>u</i>	4532 ± 1026	43	3	1	0.00	0.907	136.569
22.625	<i>u</i>	7012 ± 1280	62	0	2	0.00	0.902	136.569
22.875	<i>u</i>	8493 ± 1435	79	7	2	0.00	0.869	136.569
23.125	<i>u</i>	10557 ± 1628	88	3	1	0.00	0.839	136.569
23.375	<i>u</i>	11420 ± 1712	98	5	3	0.01	0.822	136.569
23.625	<i>u</i>	19353 ± 2280	152	4	4	0.00	0.785	136.569
23.875	<i>u</i>	20726 ± 2409	155	6	1	0.00	0.753	136.569
24.125	<i>u</i>	24928 ± 2850	160	1	6	0.00	0.647	136.569